

A Matterwave Transistor Oscillator

Seth C. Caliga, Cameron J. E. Straatsma, Alex A. Zozulya,* and Dana Z. Anderson
*Department of Physics, University of Colorado, and The JILA Institute,
 University of Colorado and National Institute for Standards and Technology, Boulder CO 80309-0440*
 (Dated: June 1, 2022)

A triple-well atomtronic transistor combined with forced RF evaporation is used to realize a driven matterwave oscillator circuit. The transistor is implemented using a metalized compound glass and silicon substrate. On-chip and external currents produce a cigar-shaped magnetic trap, which is divided into transistor source, gate, and drain regions by a pair of blue-detuned optical barriers projected onto the magnetic trap through a chip window. A resonant laser beam illuminating the drain portion of the atomtronic transistor couples atoms emitted by the gate to the vacuum. The circuit operates by loading the source with cold atoms and utilizing forced evaporation as a power supply that produces a positive chemical potential in the source, which subsequently drives oscillation. High-resolution in-trap absorption imagery reveals gate atoms that have tunneled from the source and establishes that the circuit emits a nominally mono-energetic matterwave with a frequency of 23.5(1.0) kHz by tunneling from the gate, corresponding to a vacuum energy of $2.67 \text{ MHz} \times h$, where h is Planck's constant, and a vacuum wavelength of 29 nm. Time-of-flight measurements indicate that the transistor exhibits ohmic cooling, i.e. negative resistance, and therefore has gain. Time-of-flight measurements are also used to determine an upper bound of the atomtronic transresistance, $r_m < 0.01 \text{ Hz/Hz} \times h/m^2$ where m is the mass of ^{87}Rb , and that the closed-loop circuit energy gain varies between 3.1 and 3.6.

PACS numbers: 03.75.-b, 37.10.Gh, 37.90.+j, 67.85.Hj

Keywords: Atomtronics, Matterwaves, Bose-Einstein Condensation, Atom Transistors, Tunneling, Atom Oscillators

Radiotelegraphy pioneers Alexander Meissner [1, 2] and Edwin Armstrong [3, 4] conceived of the first driven electromagnetic oscillators a century ago. Making the generation and detection of radio waves manifestly practical, the early electronic oscillators spawned an avalanche of progress in radio technology. The first inventions were electric circuits based on triode vacuum tubes, yet the class of driven oscillators evolved to include magnetrons [5], masers [6], and lasers [7], as well as many types of semiconductor device based circuits [8, 9]. The defining characteristic that distinguishes a driven oscillator from other classes is the presence of a dynamical instability—an instability that is typically intended to drive the system away from a non-oscillating equilibrium state to an oscillating one. Common among all driven oscillators are four heuristic elements: they incorporate gain and feedback in conjunction with frequency selective elements and a DC power source, e.g. a battery, to produce sustained oscillation. Here we utilize those same elements to implement an *atom* analog of a single-transistor electronic driven oscillator circuit. When appropriately coupled to an antenna or a transmission line an electronic oscillator transmits an electromagnetic wave, the energy of which is carried by photons. In an analogous fashion the atom version emits a matter wave, the energy of which is carried by atoms.

Gain in the atom-based system is provided by a triple-potential-well atomtronic transistor [10–12]. Fig. 1 shows

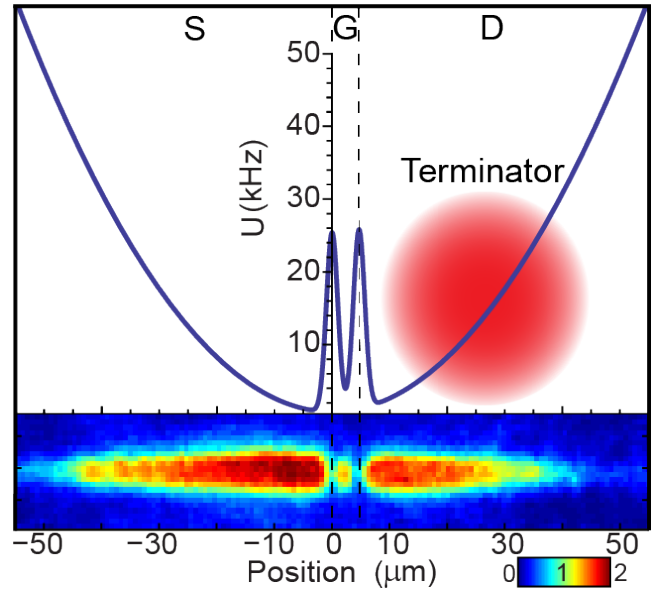


FIG. 1. The atomtronic transistor. A hybrid magnetic and optical potential creates the overall confinement of the atomic ensemble as well as a “gate” tunneling junction between “source” and “drain” wells. The upper panel shows the total longitudinal potential energy: the loose magnetic confinement along with the $4 \mu\text{m}$ $1/e^2$ full-width blue-detuned optical potential barriers separated by $4.8 \mu\text{m}$ are used to create three wells. These are labeled at the top with S, G, and D for source, gate, and drain, respectively. The terminator beam, depicted by a red circular area in the drain, out-couples atoms from the magnetic trap by optically pumping them into an untrapped m_F state. The lower panel is an in-trap absorption image of thermal atoms on an optical depth scale.

* Permanent address: Department of Physics, Worcester Polytechnic Institute, Worcester MA 01609-2280

the longitudinal profile of the potential energy surface that defines the transistor. Borrowing the nomenclature of field-effect transistors (FETs) we label the three regions of the atomtronic transistor as the “source”, “gate”, and “drain”. The bottom of Fig. 1 provides a false-color in-trap absorption image of atoms that have been loaded into the trap then subsequently cooled by RF forced evaporation to about 1 μ K. The total number of atoms is approximately 4.5×10^4 . The image reveals the three distinct regions of the transistor.

Much can be understood about the atomtronic transistor and the oscillator circuit through analogy with classical electronics by substituting chemical potential and atom flux for electrical potential and current, respectively. Electrical quantities, such as resistance, expressed in S.I. units translate to atomtronic quantities by replacing Coulombs with kilograms and the charge e of the electron with the particle mass m . This work utilizes ^{87}Rb atoms, which have a mass $m = 1.44 \times 10^{-25}$ kg. Here we will use familiar electrical symbols to represent their atomtronic analogs, except the conventional symbol μ is used for chemical potential rather than the electrical symbol V to serve as a reminder that our circuits operate with atoms rather than electrons. In Fig. 1 the zero of potential energy is taken as the bottom of the magnetic trap, although the trap bottom is biased relative to free space by $U_B = 2.645 \text{ MHz} \times h$, where h is Planck’s constant.

Quantum mechanical tunneling plays a pivotal role in atomtronic transistor behavior as it does also in a variety of semiconductor devices. In particular, tunneling provides feedback coupling between the gate and the source and is responsible for matterwave emission from the gate into the drain region. Operating with atoms electro-magnetically cooled to sub-microkelvin temperatures, two other aspects are notably different from electronic devices. First is the phenomenon of Bose-Einstein condensation (BEC) of an ensemble of atoms having integer spin, sufficiently high density, and sufficiently low temperature [13, 14]. It is through the mechanism of BEC that a positive chemical potential can be established within a well [15, 16]. Thus, an ensemble of ultracold atoms in the source well, together with forced radio-frequency (RF) evaporation that is used to induce cooling of those atoms, serves to power the circuit. Second is the quantum relationship between the energy E and the frequency f associated with an atomic wavefunction, $E = hf$. Here onward we report energy, chemical potential, and current, all in units of hertz and resistance as Hz/Hz, rather than in S.I. units, as the numerical values are rather less cumbersome for this atomtronics context. Converting to S.I. units involves multiplying an energy by h , a chemical potential by h/m , a current by m and a resistance by h/m^2 .

The atomtronic transistor is implemented using magnetic and optical fields in proximity to an atom chip comprised of a compound silicon and glass substrate. The atom chip, shown in Fig. 2, incorporates metaliza-

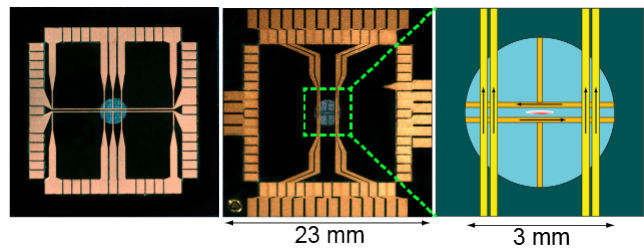


FIG. 2. Co-planar silicon and glass substrate atom microchip. The vacuum (left) and ambient (center) sides of the chip are metalized, providing conductors through which current is run to create a cigar shaped magnetic trap located 100 μm below a polished glass surface. The current scheme for this split “H”-wire trap configuration (right) produces a magnetic trap with frequencies $67 \text{ Hz} \times 1.7 \text{ kHz} \times 1.7 \text{ kHz}$.

tion for producing a cigar-shaped magnetic trap using on-chip electrical currents combined with bias fields produced by external electromagnetic coils. The window enables imaging of the atoms while they are trapped as well as projection of a pattern of light onto the trapping region [17]. In particular, the cigar-shaped magnetic trap is sliced into three separate regions by a pair of 765 nm optical barriers, that is, beams that are tuned 15 nm to the blue side of the D2 resonance of ^{87}Rb . During normal operation the drain region of the transistor is illuminated, as depicted in Fig. 1, with laser light tuned to atomic resonance. This “terminator” beam causes atoms to leave the trap; thus, atoms entering the drain from the gate are effectively coupled to the (matterwave) impedance of the vacuum.

The optical barriers play the role of the junctions between different material regions of a semiconductor device. In contrast to its electronic counterpart, the atomtronic device parameters are adjustable. In particular, the original triode tube oscillators and their transistor counterparts utilize explicit electrical elements to provide bias to the gate (or equivalent) as well as frequency selective feedback between the gate and other circuit elements. In our case bias and frequency selectivity are imposed as part of the transistor design. The barriers are produced using an acousto-optic modulator (AOM) and they are projected through the chip window using a high-resolution projection and imaging system. The width of the gate region is set by the frequency difference between a pair of RF signals driving the AOM and the barrier heights are determined by the beam intensity.

The dynamics of the transistor are largely determined by the characteristic frequencies of the three trapping regions. The longitudinal trap frequency of the gate is $\nu_g = 1.3 \text{ kHz}$ while its total ground-state energy is shifted by optical and magnetic biases to $\nu_{g0} = 6.0 \text{ kHz}$. The longitudinal frequency of the magnetic trap without the barriers is 67 Hz and therefore with the barriers the longitudinal frequency is approximately $\nu_s = 134 \text{ Hz}$ for the source and $\nu_d = 155 \text{ Hz}$ for the drain. The transverse frequencies of all three wells are approximately

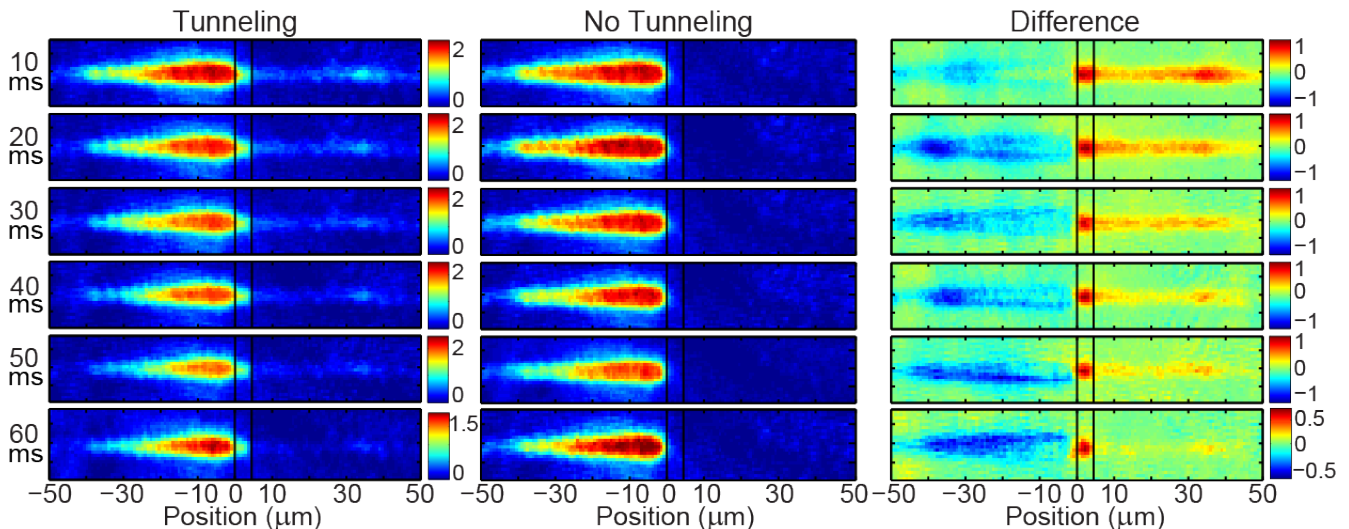


FIG. 3. A series of in-trap absorption images is taken during atomtronic circuit operation at 10 ms intervals for both tunneling allowed (left column) and tunneling disallowed (middle column) cases. Each picture is an average of 10 images taken under nominally identical conditions. The difference between the tunneling allowed and disallowed cases is shown in the right-hand column. (Note that the scale for the 60 ms case is different than the others). Vertical lines indicate the source, gate, and drain regions of the atomtronic transistor. The gate and drain become significantly populated in the tunneling allowed cases. The absorption peak at the far right of the difference images is indicative of circuit oscillation.

$\nu_t = 1.7$ kHz. Frequency selectivity of the coupling between the gate and the other two wells is largely determined by the energy eigenstates of the gate well. Given our barrier widths, tunneling of low gate energy states is negligible and only states with energies near the top of the barriers are significantly coupled.

Initialization of the circuit is carried out through a sequence of steps described in the Methods section. The preparation leaves the source well with partially condensed atoms having a predetermined chemical potential and the other two wells empty. Initialization of the circuit in this manner can be likened to charging of a capacitor attached to the source of the transistor. Subsequent circuit behavior depends on what is done with the power supply. The experiments described operate either with continuous cooling through forced evaporation by sweeping (slowly) the RF evaporation frequency, or we set the RF frequency to a fixed value, which nominally causes cooling to cease, although some residual cooling does continue. Thus, speaking very loosely we say that measurements are carried out with the power supply either set either to “on” or “trickle” after initial charging. The circuit is furthermore operated with the transistor set in one of two configurations. The “tunneling” configuration sets the barrier heights to a mean of 25.6 (1.4) kHz (individual barrier heights are different by 0.5 kHz due to their location in the magnetic trap) and the “no tunneling” configuration sets the mean to 33 kHz, which precludes any significant tunneling over the course of a measurement.

We observe circuit behavior through a series of absorption image snapshots, each taken after allowing the

circuit to operate for a given amount of time. The terminator beam is extinguished 5 ms before snapping a picture, which is somewhat less than the drain round-trip time, i.e. the classical time it takes for atoms emitted by the gate to travel up the potential of the drain well, turn around, and return to the gate. Because atoms propagate slowly at the top of their climb, the probability density is maximum near the classical turning point where the potential energy of the trap is equal to the atom’s kinetic energy. Thus, the 5 ms propagation time is sufficiently long to use the drain as a rudimentary spectrum analyzer, but sufficiently short that feedback from the drain does not dramatically impact circuit dynamics.

Fig. 3 shows a sequence of image triplets taken of the circuit operating with its power supply set to “on”. Each triplet consists of an in-trap absorption image for both the tunneling and no-tunneling modes and the third image is the difference of the first two. The difference image enables comparison between the tunneling-allowed and no-tunneling circuits and highlights features of interest. First is evidence of atoms tunneling from the source into the gate and from the gate into the drain, as indicated by the absence of atoms from the gate and the drain in the no-tunneling images. Second is the evidently substantial number of atoms in the gate. Ideally, the absorption image would provide direct information about the probability density of atoms in the wells, but our imaging system is not optimized for quantitative determination of atom number in the three wells. In fact, when the optical depth is high our in-trap absorption imaging system underestimates the atom number [18, 19].

The absorption peak that appears on the right-hand

portion of the drain well signifies circuit oscillation and matterwave emission from the gate into the drain. It is present only when tunneling is allowed, and although its intensity decreases with time its location remains approximately constant, which is indicative of transistor gain. The position of the peak corresponds to matterwave emission at an energy of $E_d = 23.2(1.0)$ kHz, or $E_v \approx 2.67$ MHz in vacuum, corresponding to a vacuum wavelength of $\lambda \approx 29$ nm.

Presuming that the output is mono-energetic and the circuit has reached dynamical equilibrium, atoms that enter and then leave the gate must have an energy that self-consistently gives rise to the gate chemical potential. In circuit language we can express the steady-state condition as

$$\frac{\mu_{sg}}{R_{sg}} = \frac{\mu_{gd}}{R_{gd}}, \quad (1)$$

where the R 's are effective junction resistances and μ_{sg} , μ_{gd} are the potential differences between the source and the gate, and the gate and the drain, respectively. We determine the source chemical potential from time-of-flight absorption imaging, [13, 19]. During oscillation the source chemical potential μ_s varies between 6.4 kHz and 7.4 kHz (see below). Depending upon circuit conditions we can suppose that the source-gate junction can be either forward ($\mu_{sg} > 0$) or reversed ($\mu_{sg} < 0$) biased during operation, and in general the resistances may be either positive or negative. A direct and dramatic consequence of the negative resistance is ohmic cooling, that is, negative power dissipation due to current flow through the effective resistance, $P_d = I^2 R$. The effect can be seen in Fig. 4, where data is taken from time-of-flight measurements. The plot shows the peak optical density of the source condensate atoms as a function of time for both tunneling and no-tunneling cases. The preparation stage is identical to that for Fig. 3 except that in this case the starting source chemical potential is lower and the power supply is operating in its trickle mode. The no-tunneling case displays a nearly constant condensate optical density as a function of time, rising a bit due to residual cooling from the fixed RF evaporation frequency. The tunneling case, however, displays an initial growth of the condensate, which indicates substantial cooling of the source atoms and an increase of its chemical potential. The density reaches a maximum and eventually falls due to the continued loss of atoms.

Negative resistance is a familiar concept in electronics, often being used to characterize gain in the oscillator context [20]. The Esaki diode is a historically significant semiconductor device for which the negative resistance arises in association with tunneling [21, 22]. In this respect, the atomtronic transistor and the tunnel diode have something in common. While the Fermi level of a semiconductor material is largely fixed, however, the chemical potentials of our transistor wells are dynamical quantities. Were it not for tunneling from the gate to the drain, thermal equilibrium would bring the source

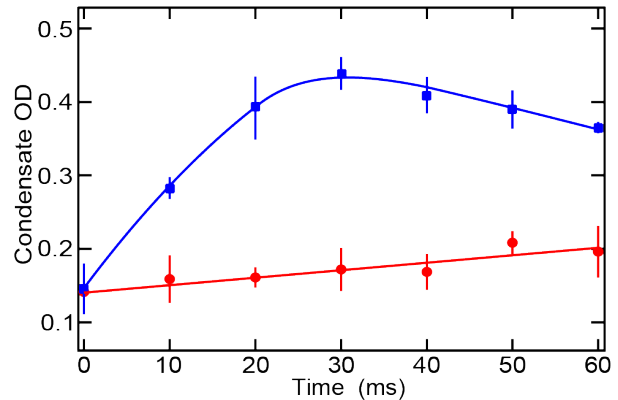


FIG. 4. Optical density of the Bose-condensate within the source well during circuit operation with the power supply in “trickle” mode. The tunneling allowed case (blue) exhibits significant cooling, whereas the tunneling forbidden case (red) shows an increase in condensate optical density due only to residual forced RF evaporation. This additional cooling corresponds to negative power dissipation. Error bars are the standard error of the mean for three measurements taken for each data point.

and gate wells to equal temperatures and chemical potentials. In the circuit, the atomtronic transistor gate has initial chemical potential equal to its ground state energy. The first atoms to tunnel from the source well are those that are most energetic. This leads to a population inversion in the gate: an unstable condition that is rapidly rectified through collisions and cooling by tunneling and/or forced evaporation of the more energetic gate atoms [23]. As atoms collect in the gate its chemical potential increases.

A handful of parameters are used to characterize a semiconductor transistor, typically specified under quiescent conditions appropriate for its intended use. In this, an oscillator context, we are concerned with the variation of output frequency with circuit parameters. We are thus particularly interested in the transresistance, as it provides the dependence of the emitted matterwave frequency on the input current. We define the atomtronic transresistance in analogy with electronics [24]:

$$r_m \equiv \frac{d\mu_{out}}{dI_{in}}. \quad (2)$$

Ideally its value is zero. The transresistance is largely governed by the inverse slope of tunneling rate through the transistor barriers as a function of particle energy. For Gaussian barriers, the tunneling rate is exponentially dependent on the incident energy, and we therefore expect the transresistance to be low. To within the measurement uncertainty of ± 1 kHz the peak energy of the emitted matterwave does not change over the course of the oscillation. The emitted current, however, changes significantly. We do not have a direct quantitative measure of the emitted current, yet we can arrive

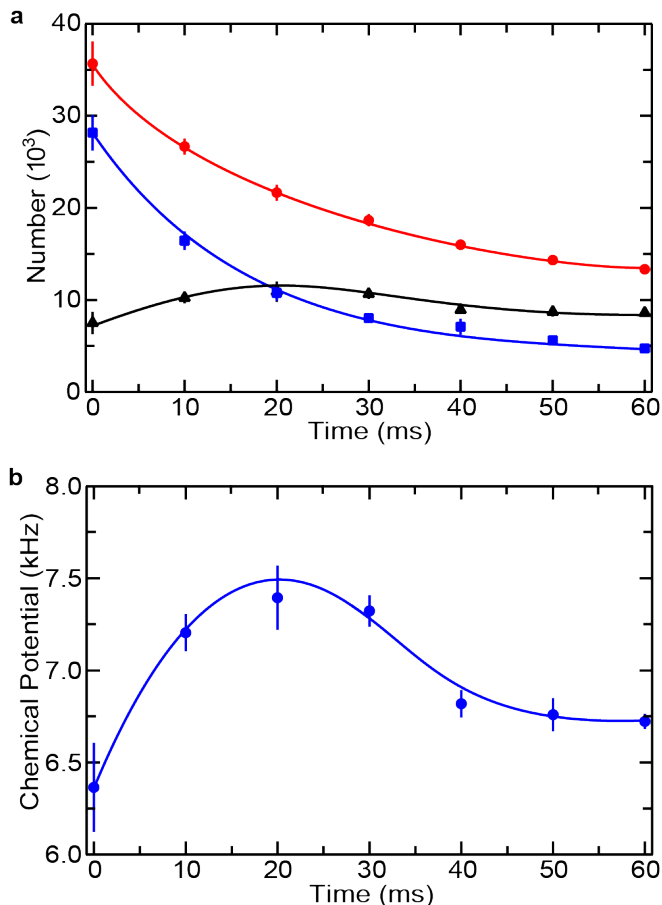


FIG. 5. a) Number of thermal (blue squares) and condensate (black triangles) as well as their sum (red circles) in the source well during circuit oscillation. b) Chemical potential of the source well during circuit oscillation. The solid curves are meant to serve as a visual aid only.

at an upper bound on the transresistance using tunneling and no-tunneling time-of-flight measurement to determine atom number in the source. Fig. 5a shows the number of atoms in the condensate and thermal components as well as their total, as a function of time under the same oscillator conditions as for Fig. 3. We assume that the fraction of atoms in the gate is a negligible contribution so that the measured atom number corresponds to those in the source well. The average current over 60 ms is $\bar{I}_T = 250$ kHz. The same measurement for the no-tunneling case $\bar{I}_{NT} = 170$ kHz. We suppose that the difference is the average drain current: $\bar{I}_d = 80$ kHz. Using the average drain current and the uncertainty for the output energy provides a rough bound on the transresistance, $r_m < 0.01$ Hz/Hz.

The chemical potential of the source, shown in Fig. 5b, can be estimated from the number of condensed atoms N_{sc} using

$$\mu_s = \frac{1}{2} \left(15N_{sc}a_s \sqrt{\frac{m\bar{v}_s}{h}} \right)^{2/5} \bar{v}_s, \quad (3)$$

where a_s is the scattering length, $a_s \simeq 5.3$ nm, and $\bar{v}_s = (\nu_s \nu_t^2)^{1/3}$. While the formula is valid for a harmonic trap, we expect that the corrections accounting for the source well geometry to be of order unity. Knowing the source potential allows us to calculate the closed-loop circuit potential gain analogous to voltage gain of an electronic circuit:

$$G \equiv \frac{E_d}{\mu_s}. \quad (4)$$

As seen in Fig. 5b, the source potential varies between 6.4 kHz and 7.4 kHz during oscillation; closed-loop gain thus varies from 3.1 to 3.6.

We have presented an atom based system that is analogous to an electronic single-transistor driven oscillator circuit. The central element is an atomtronic transistor in which the biasing as well as the frequency selectivity and feedback are incorporated by design in the transistor implementation. We have demonstrated cooling associated with tunneling in the transistor, which we have interpreted in terms of negative resistance and which indicates the availability of gain. We have calculated an upper bound for the transresistance of the device and determined the closed-loop gain for the circuit. During operation the circuit produces a nominally mono-energetic matterwave, which is a signature of driven oscillation. The instability that defines the circuit as a driven oscillator arises from the coupling of the initially unoccupied states of the gate well to occupied states of the source well. We have stated that the source atoms along with forced RF evaporation serves as our power supply. We purposefully chose the RF sweep rate so as to maintain a nominally constant source chemical potential: it is precisely the function of an electro-chemical battery to maintain a constant voltage to power an electrical circuit. The 15% variation in potential evident in Fig. 5b is, in fact, comparable to what one expects over the life of a typical carbon-zinc battery, for example [25]. Certainly our “battery” is not a very good one, as its reservoir of atoms is very finite, starting out with about 3.5×10^4 or so atoms at 750 nK. A current source continuously supplying low temperature atoms to the transistor would be ideal. There are on-going efforts to produce a practical source for continuous BEC [23, 26–30]; although technically challenging, we expect that this will be achieved. That the matterwave oscillator power supply does not require coherence among the atoms in fact relaxes some of the challenges for continuous wave operation.

We presume that the earliest driven oscillators were mechanical clocks, such as the grandfather clock that utilizes gravitational energy to sustain oscillation of a pendulum. Its operation, too, can be cast in terms of gain, feedback, frequency selective elements and a power supply. As sources of electromagnetic waves, driven oscillators of many types have left a noble legacy of technology and scientific advancement, beginning with the early days of radio. The matterwave oscillator may likewise have a significant role to play in the development of atom-based

sensors, and perhaps in quantum information processing as well.

This work is supported by AFOSR, NSF, and DARPA.

The work of S. Caliga, A. Zozulya and D.Z. Anderson was partially supported by the Charles Stark Draper Laboratories.

-
- [1] A. Meissner, “Means for Generating Electric Oscillations,” Deutsches Reich Reichspatentamt No. 291,604 (1919).
- [2] A. Meissner, “Production of Waves by Cathode Ray Tubes,” U.S. Patent No. 1,924,796 (1933).
- [3] E. H. Armstrong, “Wireless Receiving System,” U.S. Patent No. 1,113,149 (1914).
- [4] E. H. Armstrong, “Wireless Receiving System for Continuous Waves,” U.S. Patent No. 1,611,848 (1926).
- [5] H. E. Hollmann, “Magnetron,” U.S. Patent No. 2,123,728 (1938).
- [6] J. P. Gordon, H. J. Zeiger, and C. H. Townes, *Physical Review* **99**, 1264 (1955).
- [7] A. L. Schalow and C. H. Townes, *Physical Review* **112**, 1940 (1958).
- [8] M. E. V. Valkenburg and W. Middleton, *Reference Data for Engineers*, 9th ed., Radio, Electronics, Computer, and Communications (Newnes, Woburn MA, 2001).
- [9] T. C. L. G. Sollner, D. D. Tannenwald, D. D. Peck, and W. D. Goodhue, *Applied Physics Letters* **45**, 1319 (1984).
- [10] J. A. Stickney, D. Z. Anderson, and A. A. Zozulya, *Physical Review A* **75**, 013608 (2007).
- [11] R. A. Pepino, J. Cooper, D. Z. Anderson, and M. J. Holland, *Physical Review Letters* **103**, 140405 (2009).
- [12] B. T. Seaman, M. Kramer, D. Z. Anderson, and M. J. Holland, *Physical Review A* **75**, 023615 (2007).
- [13] M. H. Anderson, J. R. Ensher, M. R. Matthews, C. E. Wieman, and E. A. Cornell, *Science* **269**, 198 (1995).
- [14] M. R. Andrews, M. O. Mewes, N. J. vanDruten, D. S. Durfee, D. M. Kurn, and W. Ketterle, *Science* **273**, 84 (1996).
- [15] C. Pethick and H. Smith, *Bose-Einstein Condensation in Dilute Gases*, 1st ed. (Cambridge University Press, 2002).
- [16] R. Baierlein, *American Journal of Physics* **69**, 423 (2001).
- [17] E. A. Salim, J. DeNatale, D. M. Farkas, K. M. Hudek, S. E. McBride, J. Michalchuk, R. Mihailovich, and D. Z. Anderson, *Quantum Information Processing* **10**, 975 (2011).
- [18] G. Reinaudi, T. Lahaye, Z. Wang, and D. Guery-Odelin, *Optics Letters* **32**, 3143 (2007).
- [19] M. Pappa, Condylis, P. C., G. O. Konstantinidis, V. Bolpasi, A. Lazoudis, O. Morizot, D. Sahagun, M. Baker, and W. von Klitzing, *New Journal of Physics* **13**, 115012 (2011).
- [20] D. M. Pozar, “Microwave engineering,” (John Wiley & Sons Inc, Reading, MA, 1990) Chap. 11, 1st ed.
- [21] L. Esaki, *Physical Review* **109**, 603 (1958).
- [22] M. E. Hines and W. W. Anderson, in *1960 IEEE International Solid-State Circuits Conference. Digest of Technical Papers*, Vol. III (IEEE, 1960) pp. 12–13.
- [23] The process of loading the gate with atoms tunneling from the source is somewhat similar to the atom loading of a well described in C. F. Roos, P. Cren, D. Guery-Odelin, and J. Dalibard, *Europhysics Letters* **61**, 187 (2003).
- [24] P. Hill and W. Horowitz, *The Art of Electronics*, 2nd ed. (Cambridge University Press, 1989).
- [25] *Energcell Battery Guidebook*, 2nd ed., Radio Shack (Master Publishing, Inc., 1990).
- [26] S. Bhongale and M. Holland, *Physical Review A* **62**, 043604 (2000).
- [27] S. A. Haine, J. J. Hope, N. P. Robins, and C. M. Savage, *Physical Review Letters* **88**, 170403 (2002).
- [28] A. P. Chikkatur, Y. Shin, A. E. Leanhardt, D. Kielpinski, E. Tsikata, T. L. Gustavson, D. E. Pritchard, and W. Ketterle, *Science* **296**, 2193 (2002).
- [29] S. E. Olson, R. R. Mhaskar, and G. Raithel, *Physical Review A* **73**, 033622 (2006).
- [30] N. P. Robins, C. Figl, M. Jeppesen, G. R. Dennis, and J. D. Close, *Nature Physics* **4**, 731 (2008).
- [31] M. Razavy, *Quantum theory of tunneling* (Imperial College Pr, 2003).
- [32] L. D. Carr, M. J. Holland, and B. A. Malomed, *Journal of Physics B-Atomic Molecular and Optical Physics* **38**, 3217 (2005).

METHODS

The transistor oscillator is initialized by first loading thermal ^{87}Rb atoms into a magnetic trap located 100 μm below the surface of an atom chip. The two optical barriers separated by 4.8 μm are then swept along the weakly confined axis of the magnetic trap from the far right (see Fig. 1) towards the left to their final position by ramping the central drive frequency of the acousto-optic modulator used to produce the barriers. This loads all of the atoms into the source well of the hybrid trap. The barriers are held in place at the center of the magnetic trap as the atoms are cooled below the critical temperature using forced RF evaporation. During this evaporation the height of the barriers is lowered from 90.8 (4.9) kHz to a final height of 25.6 (1.4) kHz for the tunneling-allowed experiments. The optical intensity dependence of the barrier heights is calibrated by measuring the tunneling rate of a nominally pure condensate through a single barrier as a function of optical intensity and subsequently fitting this measured value to theoretical rates [31, 32].